Talanta 296 (2026) 128517

Contents lists available at ScienceDirect

Talanta

journal homepage: www.elsevier.com/locate/talanta

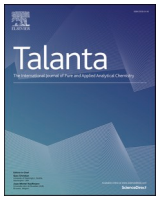

The total antioxidant capacity of fruit was determined by TAMzyme pseudo-peroxidase activity colorimetry

Xinli Guo [f,1], Shuangshuang Yan [e,1], Nishan Jin [a], Wenbin Zhong [f], Dongying An [f], Murui Ying [f], Yutian Zhou [f], Yudong Wu [e], Xin Li [b,c,d,*], Yang Zhang [a,b,**]

[a] Shenyang Key Laboratory of Medical Molecular Theranostic Probes in School of Pharmacy, Shenyang Medical College, 146 Huanghe North Avenue, Shenyang, 110034, China
[b] Liaoning Province Key Laboratory for Phenomics of Human Ethnic Specificity and Critical Illness, Shenyang Medical College, 146 Huanghe North Avenue, Shenyang, 110034, China
[c] School of Stomatology, Shenyang Medical College, Shenyang, 110034, China
[d] Shenyang Key Laboratory of Prevention and Treatment of Systemic Important Diseases Associated with Oral Diseases, Shenyang, 110034, China
[e] School of Public Health, Shenyang Medical College, 146 Huanghe North Avenue, Shenyang, 110034, China
[f] School of Basic Medicine, Shenyang Medical College, 146 Huanghe North Avenue, Shenyang, 110034, China

ARTICLE INFO

Keywords:
Nanozymes
Peroxidase-like activity
Total antioxidant capacity
Fruit
Colorimetric sensor

ABSTRACT

The total antioxidant capacity (TAC) of fruits is a key indicator for measuring their quality and nutritional value. Traditional detection methods are time-consuming and cumbersome, failing to meet the requirements for rapid detection. In this study, a novel triple metal organic framework nanozyme (TAMzyme) with superior peroxidase-like (POD-like) activity is constructed for colorimetric detection of TAC. Owing to the Fe, Co, Ni doping and unique long spindle structures, the TAMzyme possesses more surface active oxygen species, negative surface charges and rapid mass transport, thus resulting in higher catalytic activity and reaction rate. Thanks to the remarkable peroxidase-like activity, the antioxidant capacity of ascorbic acid (AA), cysteine (Cys), glutathione (Glu), and gallic acid (GA) was evaluated with a detection limit between 0.54 and 1.58 μM. Antioxidant capacity was quantified in μM Trolox Equivalent (TE), with Trolox as the standard reference compound. The sensor accurately determined the TAC in kiwi fruit (194.97 ± 2.73 μM TE) and oranges (205.10 ± 3.85 μM TE), aligning with results from a standardized ABTS kit. This study presents a rapid, cost-effective, and straightforward method for quantifying TAC in complex food matrices.

1. Introduction

In the domains of nutritional dietary guidance and health monitoring, the assessment of the holistic antioxidant capacities of fruits plays a critical role. With fruits containing a diverse array of antioxidants, the total antioxidant capacity (TAC) has become a fundamental measure for evaluating their overall antioxidant capacity [1,2]. Oxidative stress pertains to an imbalance between free radicals and antioxidants in the human body, and prolonged exposure to this imbalance can lead to cellular and tissue damage, thereby increasing the risk of various chronic health ailments [3,4]. Serving as a crucial defense mechanism in human metabolism, antioxidants neutralize free radicals, combat oxidative stress, and protect cells and organs from the harmful consequences of oxidative damage [5–7]. However, since the human body is unable to synthesize the majority of antioxidants internally, they must be refined from external sources such as fruits [8,9]. In this context, the increasing need for detailed insights into fruit antioxidants arises from the understanding that it enables individuals to make well-informed dietary decisions, leading to enhanced management of oxidative stress.

While numerous methods have been developed to assess TAC in food samples, including the 2,2′-Azinobis-(3-ethylbenzthiazoline-6-sulphonate) (ABTS) assay, 2,2′-diphenyl-1-pyridylhydrazine (DPPH) assay,

* Corresponding author. Liaoning Province Key Laboratory for Phenomics of Human Ethnic Specificity and Critical Illness, Shenyang Medical College, 146 Huanghe North Avenue, Shenyang, 110034, China.
** Corresponding author. Shenyang Key Laboratory of Medical Molecular Theranostic Probes in School of Pharmacy, Shenyang Medical College, 146 Huanghe North Avenue, Shenyang, 110034, China.
E-mail addresses: httplixin@163.com (X. Li), zhangyangpro@symc.edu.cn (Y. Zhang).
[1] These authors contributed equally to this work.

https://doi.org/10.1016/j.talanta.2025.128517
Received 15 May 2025; Received in revised form 20 June 2025; Accepted 25 June 2025
Available online 26 June 2025

Ferric Reducing Antioxidant Power (FRAP) assay, the Ferric Reducing Antioxidant Power (FRAP) assay, and electron spin resonance (ESR) spectroscopy, their methodological limitations remain poorly synthesized. A critical summary of these techniques including their operational drawbacks and technological gaps is provided inTable S1, which highlights challenges such as perishable reagents, complex instrumentation, and matrix interference commonly encountered in prior studies [10–14]. Therefore, in order to meet the practical application requirements, it is essential to develop a simpler and more user-friendly TAC measurement approach. A common strategy in TAC colorimetry employs competitive reactions, as demonstrated in both traditional ABTS systems [15] and nanozyme-based assays [16]. To achieve excellent analytical performance in this model, it is crucial to establish a robust oxidation methodology. In recent years, the benefits of nanozymes, including cost-effectiveness, exceptional stability, and straightforward preparation processes, have brought new vigor to the innovation of oxidation procedures.

Nanozymes are a class of nanomaterials exhibiting enzyme-like, capable of replicating the catalytic functions of natural enzymes on a nanoscale level [17–19]. These nanozymes not only demonstrate the high efficiency and specificity characteristic of conventional enzymes but also offer solutions to challenges such as enzyme inactivation, limited stability, and high production costs typically encountered with natural enzymes. The emergence of nanozymes has opened up new avenues and possibilities in the field of biomedicine [20–22], environmental protection [23], sterilization [24], food safety [25] and sensing [26,27].

Metal-Organic Frameworks (MOFs) are a class of porous crystalline materials formed through the self-assembly of metal ions or clusters with organic ligands, connected via coordination bonds [28,29]. These materials, characterized by their well-defined pore structure, tunable pore size, and abundant active sites, exhibit significant potential in applications such as gas adsorption and separation, catalysis, drug delivery, sensors, and energy storage [30–32]. The structural variability of MOFs stems from the wide array of metal ions and organic ligands available. Leveraging their unique catalytic activity and biocompatibility, MOF-based nanozymes can be tailored to exhibit specific enzyme functionalities, such as peroxidase (POD), catalase, superoxide dismutase, among others, through rational design of the MOF structure and composition. These nanozymes can be utilized for the elimination of detrimental substances within organisms, inflammation reduction, and facilitation of tissue repair.

In this study, we have successfully synthesized a slender spindle-shaped triple-atom-MOF nanozymes (TAMzyme) using a high-temperature hydrothermal method and utilized a colorimetric approach for the rapid and intuitive evaluation of TAC in fruits. The extensive grain and crystal surfaces of TAMzyme provide a significant specific surface area and numerous active sites, enhancing the catalytic properties of the material. Our colorimetric method is predicated on the interaction of antioxidants with H_2O_2 in the presence of TAMzyme acting as a peroxidase analog and 3,3′,5,5′-tetramethylbenzidine (TMB) serving as a chromogenic indicator. Initially, H_2O_2 is activated to generate hydroxyl radicals (•OH) on the surface of TAMzyme. Subsequently, the substrate TMB is oxidized by the hydroxyl radicals to form blue oxidized TMB (oxTMB), leading to a color change in the solution from transparent to dark blue within a few min. Throughout the detection process, the five antioxidants introduced interact with the hydroxyl radicals, competing with the TMB substrate or reducing the oxTMB [16,33], resulting in a color change in the solution that is directly proportional to the concentration of the antioxidants added. Therefore, our analytical method enables the direct quantification of antioxidant levels in fruit samples through visual inspection due to the correlation between color intensity and antioxidant concentrations.

2. Experimental section

2.1. Materials and reagents

All reagent-grade chemicals were readily accessible on the market and could be used without any additional purification steps. 2,5-Dihydroxyterephthalic acid (H_4DOT, ≥98.0 %) was purchased from Energy Chemical. Ascorbic acid (AA), glutathione (GSH), cysteine (Cys), glutamine (Gln), glucose, cobalt(II) nitrate hexahydrate ($Co(NO_3)_2{\cdot}6H_2O$, 99.99 %), nickel(II) nitrate hexahydrate ($Ni(NO_3)_2{\cdot}6H_2O$, 98 %), iron(III) nitrate nonahydrate ($Fe(NO_3)_3{\cdot}9H_2O$, 98.5 %), sodium hydroxide (NaOH), isopropyl alcohol (IPA), hydrogen peroxide (H_2O_2, 30 %), Bovine Serum Albumin, Chlorogenic Acid (CGA) and analytical-grade salts for preparing inorganic salt solutions and buffers were obtained from Sinopharm Chemical Reagent Co., Ltd. 3,3,5,5-tetramethylbenzidine (TMB) and 6-hydroxy-2,5,7,8-tetramethylchromane-2-carboxylic acid (Trolox) used in the experiments were sourced from TCI Shanghai in China. Acetic acid was purchased from Sinopharm Chemical Reagent Co., Ltd. N,N-Dimethylformamide (DMF), ethanol, and acetone were analytical-grade (AR) and obtained from Energy Chemical Industry Co., Ltd. All aqueous solutions were prepared using ultrapure water (>18 MΩ cm) generated by a Millipore system. Fruits were purchased from a local supermarket. Total Antioxidant Capacity Assay Kit (ABTS method) was purchased from Beyotime Biotechnology. Gallic acid (GA) was obtained from Aladdin Reagent Co., Ltd. (Shanghai, China).

2.2. Apparatus

X-ray diffractometer (XRD) measurements were carried out with a Bruker D8 ADVANCE X-ray diffractometer using Cu Kα1 radiation, with a scanning range between 5° and 80° using a scan step of 10°/min to evaluate the phase purity. X-ray photoelectron spectroscopy (XPS) were collected with American thermoelectric Thermo escalab 250XI. The morphology and microstructure of the materials were recorded through high resolution transmission electron microscope (HRTEM, FEI Tecnai G2 F30) and scanning electron microscopy (SEM, SU8010). Energy Dispersive Spectroscopy (EDS) was conducted using an X-MaxN detector (Oxford Instruments) coupled to a FEI Tecnai G2 F30 transmission electron microscope (300 kV). Ultraviolet analysis was performed on the UV–vis Spectrophotometer F-7000 (PERSEE, Beijing) and Microplate Reader (BioTek CYTATION 5, USA). The small juicer cup was purchased from NanJiren Kitchen Appliances Flagship Store.

2.3. The synthesis of the TAMzyme

A solution containing 21 mM of $Fe(NO_3)_3{\cdot}9H_2O$, 21 mM of $Co(NO_3)_2{\cdot}6H_2O$, 21 mM of $Ni(NO_3)_2{\cdot}6H_2O$, and 24 mM of H_4DOT was prepared by dissolving them in 5 mL of water. Subsequently, 75 mL of DMF and 5 mL CH_3CH_2OH were added to this solution. The mixture was then stirred magnetically for 30 min. Following this, the solution was transferred to a Teflon-lined stainless steel container and heated at 120 °C for 24 h. After cooling, the resulting products were subjected to centrifugation, washed three times with acetone, and vacuum-dried at 60 °C for 24 h, resulting in the formation of TAMzyme.

2.4. Analysis of peroxidase mimetic activity

The POD-like activity of TAMzyme was assessed using a colorimetric method with TMB as the substrate. In an acetic acid-sodium acetate buffer solution (pH = 3.0, 170 μL), a sequential addition of H_2O_2 (5 mM, 10 μL), TMB substrate (0.5 mM, 10 μL), and TAMzyme (1 μg/mL, 10 μL) was made and incubated for 30 min. Subsequently, the absorbance values of the reaction system at 652 nm were measured using a UV–vis spectrophotometer. Following this, the peroxidase-like activity of TAMzyme was examined under various conditions, including pH values

(2–12), catalytic reaction time (1, 6, 10, 15, 20, 30, 50, and 60 min), temperatures (4, 10, 20, 25, 30, 37, 40, 50, and 60 °C), and TAMzyme concentrations (0.1, 0.5, 0.8, 1.0, 1.5, 2.0, 2.5, 3.0, and 4.0 μg/mL), aiming to optimize the performance of TAMzyme for further investigations.

2.5. Kinetics

The steady-state kinetic assay was performed in a NaAc-HAc buffer (pH = 3.0, 0.1 M) using 10 μL of TAMzyme (1 μg/mL). The initial concentrations of TMB (0, 0.1, 0.25, 0.5, 0.75, 1.0, and 1.25 mM) or H_2O_2 (0, 0.5, 0.75, 1.0, 2.5, 5, 10, 15, and 20 mM) were set under the optimized conditions (pH = 3.0, T = 40 °C). The absorbance at 652 nm of the resulting solution was recorded. The *Michaelis-Menten* equation was applied, and kinetic parameters were calculated by using the *Lineweaver-Burk* plot equation: $1/v = K_m/(v_{max}[S]) + 1/v_{max}$, where v signifies the initial velocity of the reaction, v_{max} represents the maximum achievable velocity, *[S]* denotes the concentration of the substrate, and K_m signifies the *Michaelis-Menten* constant.

2.6. The reusability of the TAMzyme

The reusability of nanozyme was evaluated through cyclic catalytic experiments. In a 600 μL system, a mixture of TMB (0.5 mM, 30 μL) solution and H_2O_2 (5 mM, 30 μL) solution with TAMzyme (1 μg/mL, 30 μL) was reacted at pH = 3 and 40 °C for 30 min. The absorbance at 652 nm was recorded as A_0. Following the reaction, TAMzyme was separated by centrifugation (10000 rpm, 20 min), washed twice with absolute ethanol and once with distilled water. Fresh TMB and H_2O_2 solutions were added, and the reaction was repeated for 6 cycles, with the absorbances of each cycle recorded as A_1, A_2, …, A_6. The activity retention rate (R) was determined using the formula: $R = (A_n/A_0) \times 100$ %, where A_0 is the initial absorbance at 652 nm, and A_n is the absorbance recorded in the nth cycle.

2.7. Catalytic mechanism

The catalytic mechanism of TAMzyme in POD-like activity was investigated by employing IPA scavengers to eliminate •OH. A 600 μL reaction solution was prepared by combining 30 μL IPA (0–4 mM), 30 μL H_2O_2 (5 mM), 30 μL TMB (0.5 mM), and 30 μL TAMzyme (1 μg/mL) in 480 μL NaAc-HAc buffer (pH = 3.0). Following a 40-min incubation at 40 °C, the UV–vis absorption spectrum was recorded within the range of 450–750 nm to analyze the reaction.

2.8. TAMzyme-based sensing strategies for antioxidants

To demonstrate the capability of the system to detect a variety of antioxidants, TAMzyme (1 μg/mL, 10 μL) was dispersed in a 200 μL of reaction mixture containing TMB (0.5 mM, 10 μL), H_2O_2 (5 mM, 10 μL), and NaAc-HAc buffer (pH = 3.0). The absorbance values were monitored for five different antioxidants at varying concentrations: AA (5–70 μM), Cys (2–100 μM), GSH (1–100 μM), GA (1–200 μM), and Trolox (1–300 μM). After incubating at 40 °C for 30 min, the absorbance at 652 nm was measured. The Limit of Detection (LOD) and Limit of Quantitation (LOQ) for the antioxidants were determined using the formulas: $LOD = 3\sigma/k$, $LOQ = 10\sigma/k$, where σ represents the standard deviation of the blank group consisting of 10 samples, and k denotes the gradient between the absorbance values measured at 652 nm and the content of antioxidants.

2.9. Fruits sample treatment and validation assay

Fresh kiwi fruits and oranges are procured from local grocery stores. Initially, 30.0 g of peeled fresh kiwi fruit or orange is mechanically crushed using a juicer and filtered through a filter bag to obtain juice. The fresh juice is then diluted with deionized water to reach a final volume of 50 mL. In a 200 μL total system, the absorbance at 652 nm is determined by mixing 10 μL TAMzyme (1 μg/mL) with NaAc-HAc buffer (pH = 3.0, 0.1 M), TMB (0.5 mM, 10 μL), H_2O_2 (5 mM, 10 μL), and solutions of various concentrations of Trolox in a 96-well plate. Subsequently, the Trolox equivalent value is calculated to establish a standard curve. Following this, a mixture of 10 μL of juice solution (Trolox dosage 0, 50, 100, 150 μM), 10 μL TAMzyme (1 μg/mL), 10 μL TMB (0.5 mM), 10 μL H_2O_2 (5 mM), and 160 μL buffer is prepared and incubated at 40 °C for 30 min, after which the absorbance at 652 nm is measured.

3. Results and discussion

3.1. Characterization of the synthesized TAMzyme

Multimetallic MOF-74 materials were synthesized via a simple one-pot solvothermal method using divalent metal ions and H_4DOT. The SEM image (Fig. 1A) and HR-TEM image (Fig. 1B) reveal the uniformly dispersed long spindle shape of TAMzyme. The energy-dispersive system's mapping image (Fig. 1C and D) demonstrates a homogeneous distribution of Fe, Co, Ni, C and O throughout the samples. Additionally, the analysis of the energy-dispersive spectroscopy (EDS) data indicates that the relative content percentages of Fe, Co, Ni, C and O are 2.20 %, 4.33 %, 4.14 %, 49.86 %, and 39.47 %, respectively. For a more comprehensive understanding of the chemical composition and state of the sample, X-ray photoelectron spectroscopy (XPS) was utilized to investigate the electronic structure and elemental valence states of TAMzyme. The XPS spectrum (Fig. 1Ea) confirms the presence of Fe, Co, Ni, C, and O elements in the sample.

High-resolution XPS analysis of the C 1s spectrum (Fig. 1Eb) reveals a distinct peak centered at 284.8 eV, indicative of the C–C bond, confirming the presence of amorphous carbon in the sample. The additional peaks observed at 286.88 eV and 288.48 eV are attributed to the presence of C–O and O–C═O chemical bonds [34]. The peak observed in the O 1s spectrum at 529.78 eV corresponds to the (FeCoNi)–O bond (Fig. 1Ec). Furthermore, the binding energies recorded at 531.69 eV and 533.68 eV suggest the presence of chemical bonds between carbon- and oxygen-containing groups on the metal oxide surface, specifically the C–O and –O–C═O linkages [35]. The Fe 2p spectrum, illustrated in Fig. 1Ed, displays a division into three distinct peaks. The peaks observed at 711.57 eV and 724.08 eV signify the presence of Fe^{2+}. The peak at 716.18 eV is associated with a satellite peak, which is related to the oscillatory excitation phenomenon observed in high-spin Fe^{2+} states [36,37]. In the Co 2p spectrum depicted in Fig. 1Ee, the peaks centered at 781.41 eV and 797.08 eV correspond to the Co 2p3/2 and Co 2p1/2 electrons of Co^{2+}. Additionally, satellite peaks are observed at 785.88 eV and 801.98 eV [38]. Subsequently, the resolution of the Ni 2p spectral data (Fig. 1Ef) reveals two distinct Ni states: Ni^{2+} and satellites. The prominent peaks detected at 860.78 eV and 878.38 eV are attributed to satellite peaks, while the binding energies measured at 856.38 eV and 873.28 eV indicate the Ni 2p3/2 and Ni 2p1/2 electron states, respectively [39]. The X-ray diffraction (XRD) analysis conducted on TAMzyme revealed a crystalline structure, with diffraction peaks aligning well with the simulated MOF-74 crystalline structure, as depicted in Fig. S1. Therefore, it can be concluded that achieved TAMzyme with the trimetallic MOF structure.

3.2. POD-like activity of TAMzyme

Among the diphenylamine substrates commonly utilized in POD assays, TMB demonstrates the highest sensitivity, superior purity of colored product, and reasonable stability of the oxidized product [40]. Consequently, we assessed the POD-like activity of TAMzyme under a nitrogen atmosphere using TMB as the color-developing substrate. The findings revealed that, in the presence of H_2O_2, TAMzyme facilitated the oxidation of the colorless TMB to the blue oxTMB, exhibiting a

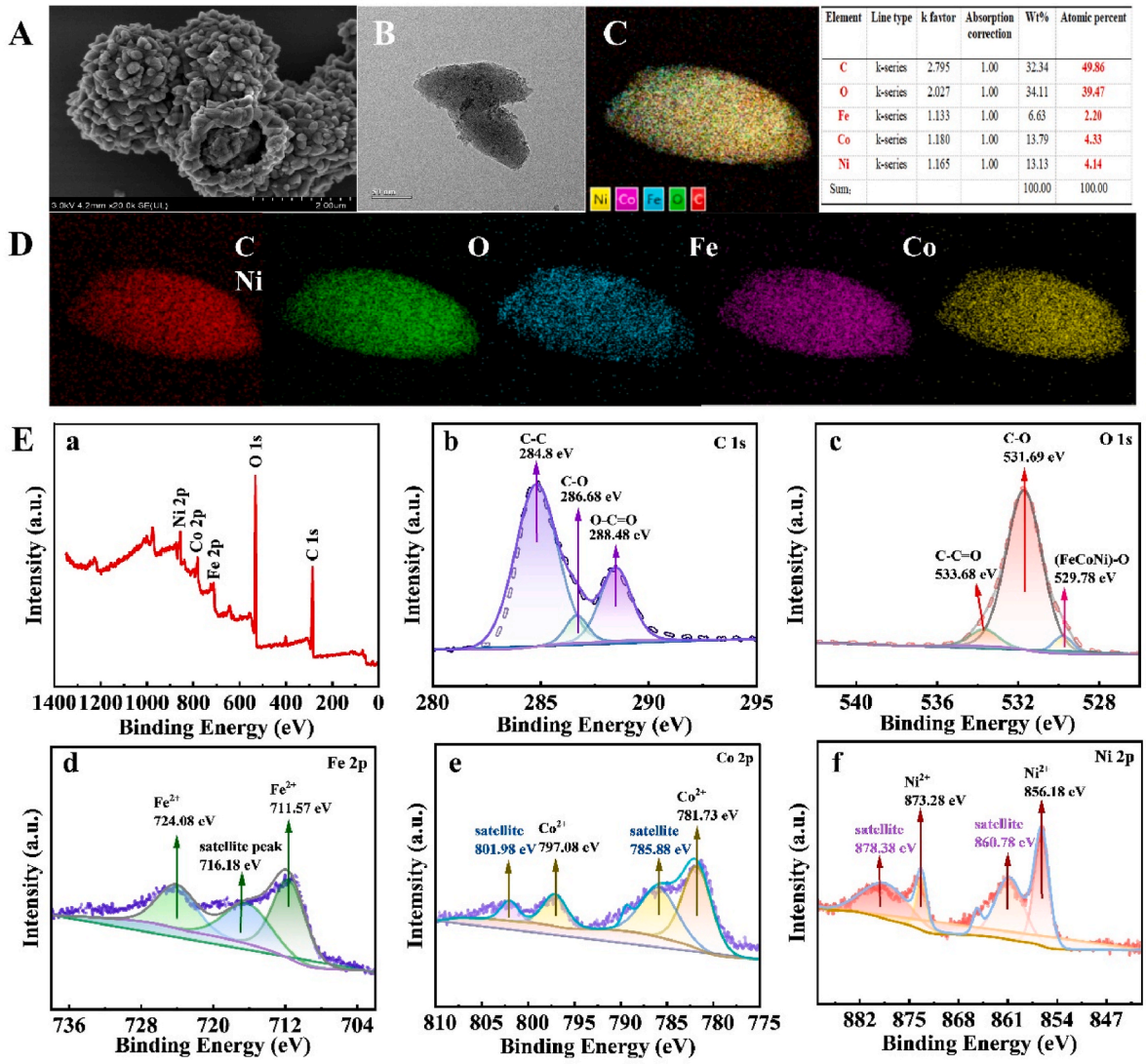

Fig. 1. (A) SEM image. (B) HR-TEM image. (C, D) the corresponding elemental mappings distribution of TAMzyme, showing the hierarchical elemental distributions of C, O, Ni, Co and Fe. (E) XPS spectra of TAMzyme: (a) XPS-survey, (b) C 1s spectrum, (c) O 1s spectrum, (d) Fe 2p spectrum, (e) Co 2p spectrum, and (f) Ni 2p spectrum.

maximum absorbance peak at 652 nm (Fig. 2A).

To gain a deeper insight into the key factors influencing substrate oxidation, various parameters including pH, temperature, catalytic reaction time, and TAMzyme concentration were evaluated. With an increase in pH from 2 to 12, the absorbance of the oxidized substrate peaked at pH = 3.0, highlighting the exceptional catalytic performance of TAMzyme under acidic conditions, particularly at pH = 3.0 (Fig. 2B). Significantly, at pH levels exceeding 5.0, TAMzyme experiences a substantial decrease in activity, highlighting its inadequacy for weakly acidic environments. The enhanced POD-like activity of TAMzyme under acidic conditions was primarily attributed to the surface charge effect: in acidic environments (where the pH was lower than the isoelectric point of the nanozyme), the nanozyme surface carries a positive charge (Fig. S2). In solution, H_2O_2 dissociates into HO_2^- and H^+, and the negatively charged HO_2^- is more readily adsorbed onto the positively charged surface of the nanozyme. This enhances the binding efficiency between the substrate and the active site, thereby accelerating the catalytic reaction. In Fig. 2C, the absorbance of the system (TAMzyme, H_2O_2, and TMB) at 652 nm increases as the temperature is elevated from 4 °C to 40 °C before reaching a plateau, indicating the wide temperature range over which TAMzyme can effectively operate. In Fig. 2D, it is evident that the absorbance of the system shows a rapid increase from 1 min to 30 min, after which it stabilizes with prolonged reaction time, indicating a corresponding increase and eventual stabilization of oxTMB. A similar pattern was observed when the catalytic reaction was conducted at varying concentrations (Fig. 2E). As the TAMzyme concentration reached a plateau, the absorbance at 652 nm showed a gradual increase, suggesting an optimal TAMzyme concentration of 1 μg/mL. However, it is important to note that H_2O_2 is prone to decomposition under alkaline conditions and elevated temperatures, resulting in a decrease in the absorbance of the catalytic system.

To investigate the mechanism of this catalytic reaction, the generation of •OH in the catalytic process was confirmed using IPA. Due to the strong affinity between the hydroxyl group (-OH) of IPA and •OH, •OH preferentially reacts with the hydroxyl group of IPA upon encountering it. Additionally, IPA reacts with •OH to form relatively stable intermediates, which may undergo further transformation or degradation. In Fig. 2F, as the concentration of IPA increases, the absorbance of the TAMzyme/H_2O_2/TMB system gradually decreases in the range of 450–750 nm, indicating that H_2O_2 is catalytically decomposed by TAMzyme to generate·OH.

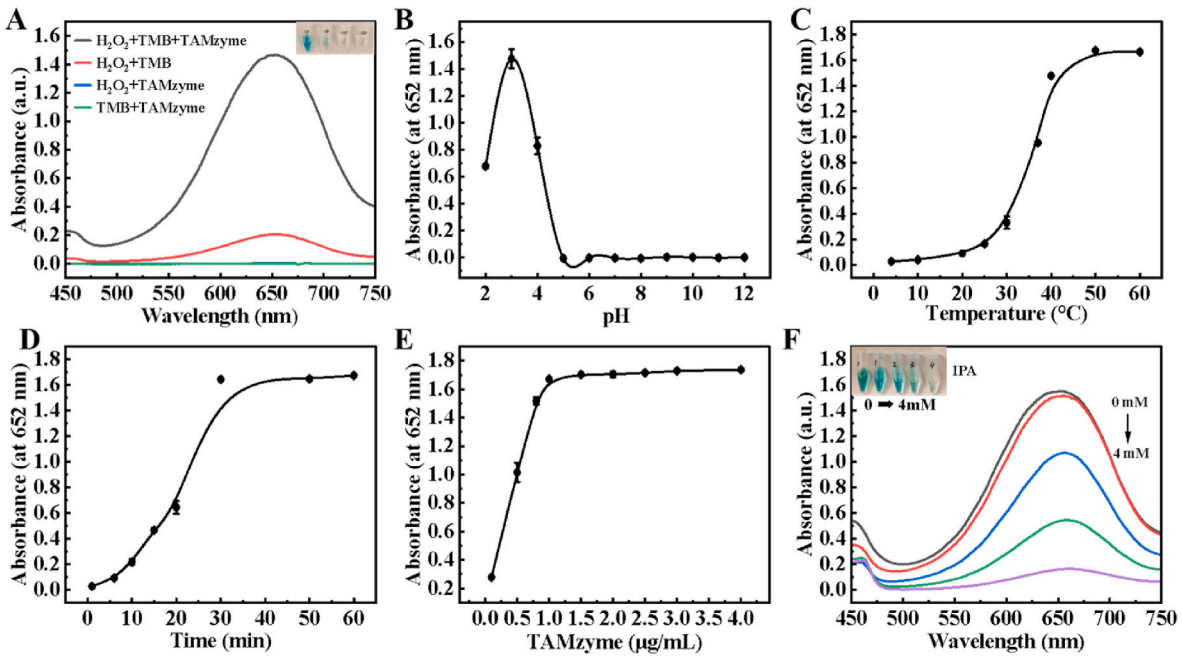

Fig. 2. (A) POD-like activity: typical absorption spectra of TMB, oxidationcatalyzed by TAMzyme and control groups in the presence of H_2O_2 at pH 3.0. (B) pH 2–12. (C) Temperature (4 °C–60 °C). (D) Reaction time (1–60 min). (E) Concentration (0.1–4.0 μg/mL) of TAMzyme. (F) The absorption spectrum of IPA as a scavenger for •OH.

3.3. Steady-state kinetics of the TAMzyme

Steady-state kinetics experiments demonstrated a significant increase in the catalytic reaction rate as the concentrations of the TMB and H_2O_2 substrates were increased, eventually reaching a saturation point. Importantly, the catalytic reaction followed the *Michaelis-Menten* kinetic model, as illustrated in Fig. 3A and C. Detailed analysis of the double reciprocal *Lineweaver-Burk* plot revealed that the *Michaelis-Menten* constant (K_m) for TMB substrate stood at 0.1115 mM (Fig. 3B), while for H_2O_2 substrate, it was 1.4857 mM (Fig. 3D). These results indicate that TAMzyme exhibits strong substrate affinity and exceptional catalytic activity (Table S2).

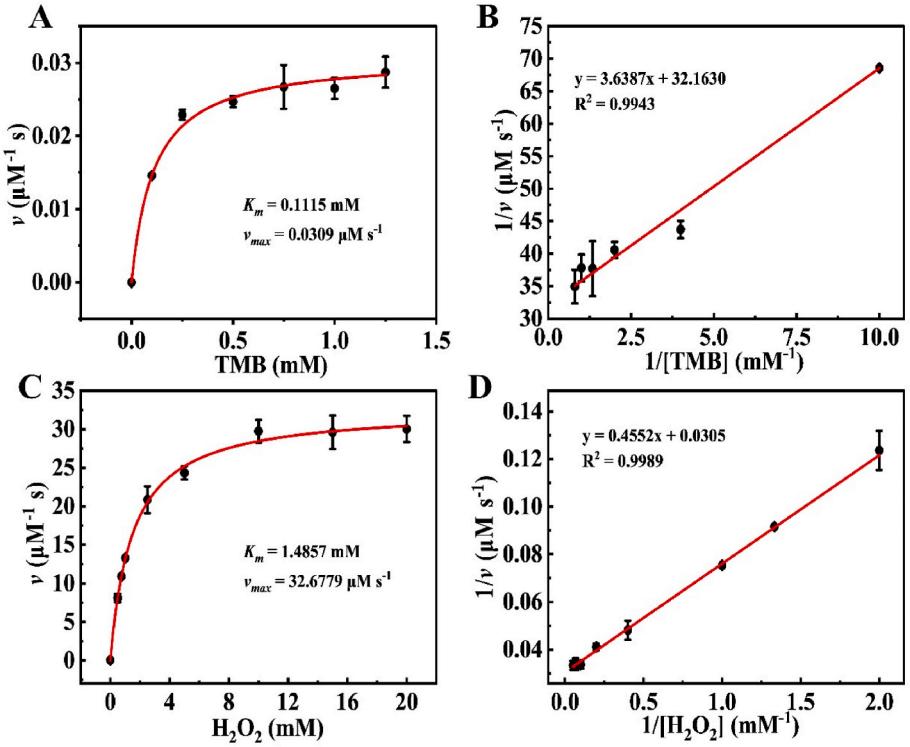

Fig. 3. (A) The concentration of H_2O_2 was 5 mM and the TMB concentration varied. (B) Double reciprocal plots of the *Michaelis-Menten* equation from the activity date of the concentration of TMB. (C) The concentration of TMB was 0.5 mM and the H_2O_2 concentration varied. (D) Double reciprocal plots of the *Michaelis-Menten* equation from the activity date of the concentration of H_2O_2.

3.4. Reusability evaluation of the TAMzyme

The recyclability of catalysts is crucial for continuous operation and cost efficiency. In this study, the TAMzyme was evaluated for its recyclability over six cycles. After each 20-min cycle, the product was separated via centrifugation, and the reaction system was replenished with fresh substrate. Throughout the six cycles, approximately 80 % of the initial activity was retained, as shown in Fig. S4 and Table S3. The decrease in activity can be attributed to particle loss during centrifugation, a challenge to quantify accurately. Nevertheless, the TAMzyme demonstrates excellent recyclability, making it suitable for practical applications.

3.5. TAMzyme-based sensing strategies for antioxidants

The performance of the TAMzyme-based sensing system was assessed by detecting antioxidants such as AA, Cys, GSH, GA and Trolox, which can act as the main components of TAC in fruits. Fig. 4A-D illustrate an increase in antioxidant concentration led to a decrease in the absorbance of the system, indicating that antioxidants exhibited a certain inhibitory effect on the oxidation of TMB [33]. Furthermore, the variation in net absorbance values at 652 nm in relation to antioxidant concentration, offering a quantitative evaluation of the response of the colorimetric methods to the target antioxidant concentrations. The change in absorbance value shows a clear linear correlation with the concentrations of four antioxidants. Linear calibration curves were established based on the TAMzyme-TMB colorimetric approach, with the LOD for the aforementioned antioxidants ranging from 0.54 to 1.58 μM, and the LOQ ranging from 1.81 to 5.27 μM (Table S4). Therefore, the developed TAMzyme exhibits promising application potential.

Trolox, a commonly used antioxidant, serves as a standard for evaluating the TAC of various antioxidants. The TAC of the samples is expressed as μM Trolox Equivalent (TE). In this system, the oxidation of TMB is hindered by the reaction of Trolox by •OH radicals, leading to a gradual decrease in absorbance of the working solution with increasing Trolox concentration. The absorbance at 652 nm exhibited a linear relationship with Trolox concentrations ranging from 1 to 300 μM, as shown in Fig. 4E, with an equation of $y = -1.6019x + 0.6360$ and an R^2 value of 0.9943. The method demonstrated effectiveness in Trolox detection, with a LOD of 0.53 μM and a LOQ of 1.77 μM.

Furthmore, the selectivity of the TAMzyme hybrid system was evaluated against inorganic ions at 1 mM (K^+, Na^+, Mg^{2+}, Cu^{2+}, Zn^{2+}, SO_4^{2-}, and NO_3^-) and organic molecules at 200 μM (AA, GSH, Cys, Gln, Glusose, Protein, and CGA) (Fig. S3). In the presence of antioxidant compounds, notable changes in absorbance were observed, indicating high sensor selectivity with minimal interference from other substances.

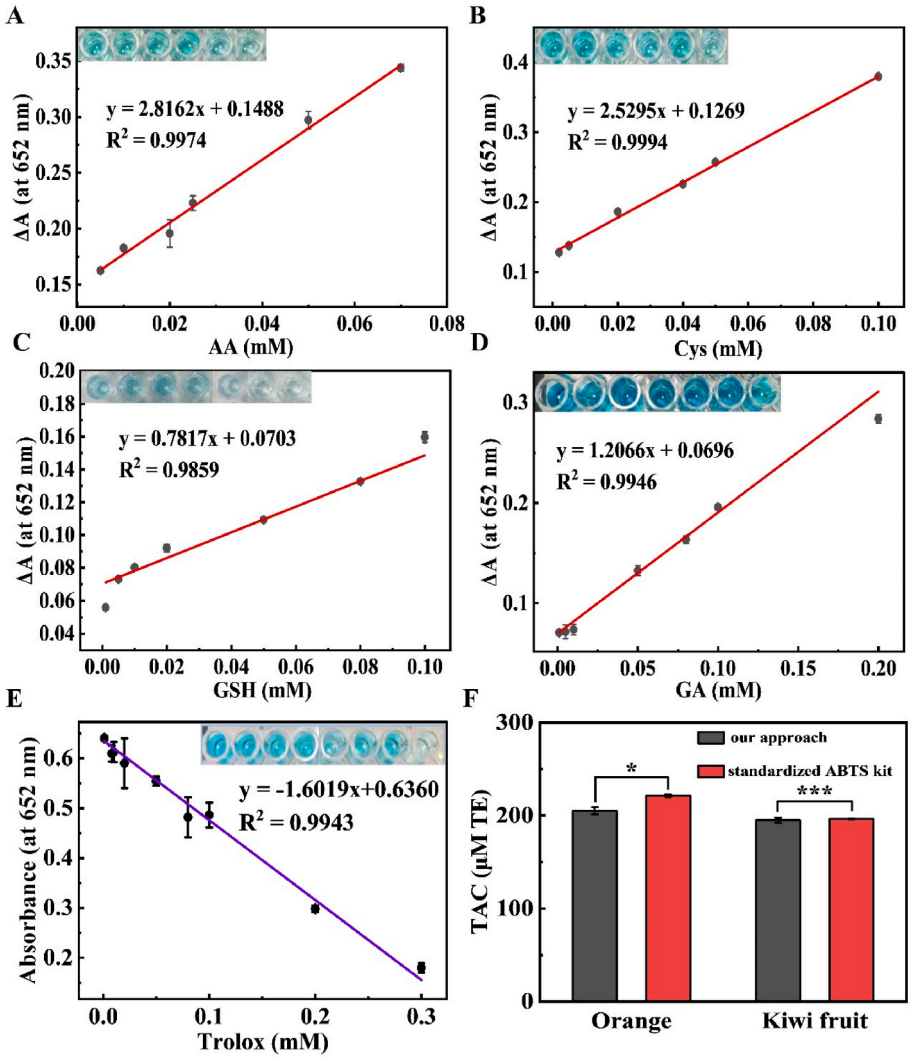

Fig. 4. TAMzyme-based sensing strategy was used for the detection of (A) AA, (B) Cys, (C) GSH, and (D) GA. Using TMB as substrate, the calibration diagram were obtained. (E) The linear relationship between the absorbance at 652 nm and concentrations of Trolox. (F) Comparison of TAC detection in two samples using the TAMzyme-based colorimetric assay and the standardized ABTS kit. Data are shown as mean ± SD (*$p < 0.05$, **$p < 0.01$, and ***$p < 0.001$).

Given that Trolox can interact with •OH to diminish oxTMB production, the reduced product can be accurately quantified.

3.6. Measurement of TAC levels in fruits

To evaluate the efficacy of the TAMzyme-based colorimetric assay in practical samples, two fresh fruits were selected for juicing and their TAC was evaluated. A standard curve was generated using Trolox as a control, and the test results were expressed in Trolox equivalent (μM). As shown in Table 1, the TAC of kiwi fruit was determined to be 194.97 ± 2.73 μM TE, while that of oranges was measured at 205.10 ± 3.85 μM TE, indicating robust antioxidant activity beneficial for daily dietary planning. To ensure the accuracy of our proposed method, the standard addition method was employed, and the recovery was calculated. The recovery rates for kiwi fruit samples ranged from 98.97 % to 108.30 %, while those for orange samples ranged from 88.48 % to 101.28 %, demonstrating the excellent accuracy of the TAMzyme-based sensing approach. In addition, a comprehensive comparison was made between the TAMzyme-based colorimetric method and other nanoparticle-based nanozyme techniques (Table S5), demonstrating its remarkably low detection limit (1.41 μM for Trolox) and satisfactory recovery range (88.48–108.30 %), which ensure the precision and reliability of TAC determination across diverse fruit samples and concentration levels. This nanozyme-based sensor exhibits promising potential for sensitivity and precise quantification of TAC in practical fruit samples.

In this work, the TAC of kiwi fruit and oranges was measured using the TAMzyme-based colorimetric assay and compared with the results obtained from a standardized ABTS kit (Fig. 4F and Table 2). For kiwi fruit and oranges, the TAC values determined by the TAMzyme-based colorimetric assay were 194.97 ± 2.73 μM TE and 205.10 ± 3.85 μM TE, respectively. These results showed good agreement with those obtained from the standardized ABTS kit (196.43 ± 0.54 μM TE for kiwifruit and 221.39 ± 1.41 μM TE for oranges), indicating that the TAMzyme-based colorimetric assay has acceptable accuracy and repeatability compared to the conventional method for measuring the TAC of these two plant-derived samples.

Table 1
Recovery test and precision of the determination of TCs in real samples by colorimetric sensor.

Sample	Tatal found equivalents of Trolox (μM)	Added Trolox (μM)	Detected equivalents of Trolox (μM)	Recovery (%)	RSD (%,n = 3)
Kiwi fruit	194.97 ± 2.73	50	105.19 ± 1.08	98.97	2.77
		100	157.71 ± 2.54	102.00	1.81
		150	218.16 ± 0.93	108.30	0.13
Orange	205.10 ± 3.85	50	89.41 ± 1.06	88.48	0.95
		100	146.45 ± 2.63	101.28	3.01
		150	188.42 ± 1.07	95.50	0.59

Table 2
Comparative study of TAC detection in fruits using the proposed TAMzyme-based colorimetric strategies and a standardized ABTS kit.

Samples	TAMzyme-based colorimetric assay (μM, Mean ± SD)	ABTS kit (μM, Mean ± SD)
Kiwi fruit	194.97 ± 2.73	196.43 ± 0.54
Orange	205.10 ± 3.85	221.39 ± 1.41

4. Conclusions

The study introduces a one-step self-assembly approach for synthesizing a novel TAMzyme with elongated spindle-like morphology and remarkable POD-like activities, offering a viable alternative to natural enzymes for assessing the TAC of food samples. The colorimetric sensing strategies based on TAMzyme provide distinct advantages over natural enzymes, such as cost and time efficiency in production, resilience to denaturation under harsh conditions, and support for large-scale implementation of the TMB method for TAC analysis. By combining TAMzyme with TMB to develop a colorimetric sensor, we have successfully achieved highly sensitive and accurate TAC detection in two types of fruits using Trolox as a reference standard. Comparative assessments on two kinds of fruit varieties underscore the promising application of TAMzyme-based sensing strategies for TAC determination in food samples. The study currently focuses on a limited range of fruit samples and does not differentiate the contributions of individual antioxidant components. In future work, we aim to expand the sample diversity and integrate multi-technique analysis to address these gaps, while optimizing the detection protocol for broader practical applications.

CRediT authorship contribution statement

Xinli Guo: Writing – original draft, Methodology, Investigation, Data curation. **Shuangshuang Yan:** Writing – original draft, Methodology, Investigation, Data curation. **Nishan Jin:** Investigation. **Wenbin Zhong:** Investigation. **Dongying An:** Investigation. **Murui Ying:** Methodology. **Yutian Zhou:** Investigation. **Yudong Wu:** Supervision. **Xin Li:** Supervision, Funding acquisition. **Yang Zhang:** Writing – review & editing, Supervision, Funding acquisition, Conceptualization.

Declaration of competing interest

The authors declare that they have no known competing financial interests or personal relationships that could have appeared to influence the work reported in this paper.

Acknowledgments

The authors appreciate financial supports from the Shenyang Science and Technology Talent Special Project (RC230022), Liaoning Provincial Department of Education (LJ222100164024, LJ222100164030), Liaoning Province Science and Technology Joint Plan (2024JH2/102600237), Natural Science Foundation Joint Fund of Liaoning Province (2023-MSLH-288), Shenyang Medical College Project (SYKT2025002, SYKT2025004, SYKT2025005 and SYKT2025007).

Appendix A. Supplementary data

Supplementary data to this article can be found online at https://doi.org/10.1016/j.talanta.2025.128517.

Data availability

Data will be made available on request.

References

[1] D. Guo, C. Li, G. Liu, X. Luo, F. Wu, Oxidase mimetic activity of a metalloporphyrin-containing porous organic polymer and its applications for colorimetric detection of both ascorbic acid and glutathione, ACS Sustainable Chem. Eng. 9 (2021) 5412–5421.
[2] X. Zhou, M. Wang, X. Su, Sensitive glutathione S-transferase assay based on Fe-doped hollow carbon nanospheres with oxidase-like activity, Sensor Actuat B-Chem. 338 (2021) 129777.
[3] L.U. Pagan, M.J. Gomes, M. Gatto, G.A.F. Mota, K. Okoshi, M.P. Okoshi, The role of oxidative stress in the aging heart, Antioxidants 11 (2022) 336.
[4] R. Singh, S. Devi, R. Gollen, Role of free radical in atherosclerosis, diabetes and dyslipidaemia: larger-than-life, Diabetes Metabolism Res 31 (2015) 113–126.
[5] H.J. Forman, H. Zhang, Targeting oxidative stress in disease: promise and limitations of antioxidant therapy, Nat. Rev. Drug Discov. 20 (2021) 689–709.
[6] W. Wang, P.M. Kang, Oxidative stress and antioxidant treatments in cardiovascular diseases, Antioxidants 9 (2020) 1292.
[7] V. Unsal, M. Cicek, İ. Sabancilar, Toxicity of carbon tetrachloride, free radicals and role of antioxidants, Rev. Environ. Health 36 (2021) 279–295.

[8] L.-T. Sheng, Y.-W. Jiang, L. Feng, A. Pan, W.-P. Koh, Dietary total antioxidant capacity and late-life cognitive impairment: the Singapore Chinese health study, J Gerontol A-Biol 77 (2022) 561–569.
[9] N. Stedile, R. Canuto, C.D. de Col, J.S. de Sene, A. Stolfo, G.N. de S. Wisintainer, J. A.P. Henriques, M. Salvador, Dietary total antioxidant capacity is associated with plasmatic antioxidant capacity, nutrient intake and lipid and DNA damage in healthy women, Int. J. Food Sci. Nutr. 67 (2016) 479–488.
[10] Q. Hu, H. Sun, X. Zhou, X. Gong, L. Xiao, L. Liu, Z. Yang, Bright-yellow-emissive nitrogen-doped carbon nanodots as a fluorescent nanoprobe for the straightforward detection of glutathione in food samples, Food Chem. 325 (2020) 126946.
[11] D. Li, J. Jiang, D. Han, X. Yu, K. Wang, S. Zang, D. Lu, A. Yu, Z. Zhang, Measurement of antioxidant capacity by electron spin resonance spectroscopy based on Copper(II) reduction, Anal. Chem. 88 (2016) 3885–3890.
[12] I.G. Munteanu, C. Apetrei, Analytical methods used in determining antioxidant activity: a review, IJMS 22 (2021) 3380.
[13] M. Ozgen, R.N. Reese, A.Z. Tulio, J.C. Scheerens, A.R. Miller, Modified 2,2-Azino-bis-3-ethylbenzothiazoline-6-sulfonic acid (ABTS) method to measure antioxidant capacity of selected small fruits and comparison to ferric reducing antioxidant power (FRAP) and 2,2‘-Diphenyl-1-picrylhydrazyl (DPPH) methods, J. Agric. Food Chem. 54 (2006) 1151–1157.
[14] M. Plaza, J. Kariuki, C. Turner, Quantification of individual phenolic compounds’ contribution to antioxidant capacity in apple: a novel analytical tool based on liquid chromatography with diode array, electrochemical, and charged aerosol detection, J. Agric. Food Chem. 62 (2014) 409–418.
[15] R. Re, N. Pellegrini, A. Proteggente, A. Pannala, M. Yang, C. Rice-Evans, Antioxidant activity applying an improved ABTS radical cation decolorization assay, Free Radical Biol. Med. 26 (1999) 1231–1237.
[16] D. Pedone, M. Moglianetti, M. Lettieri, G. Marrazza, P.P. Pompa, Platinum nanozyme-enabled colorimetric determination of total antioxidant level in saliva, Anal. Chem. 92 (2020) 8660–8664.
[17] J. Chang, L. Yu, T. Hou, R. Hu, F. Li, Direct and specific detection of glyphosate using a phosphatase-like nanozyme-mediated chemiluminescence strategy, Anal. Chem. 95 (2023) 4479–4485.
[18] X. Sang, An efficient enzyme cascade bio-platform based on metal-organic frameworks nanozyme for the detection of glucose, J Chinese Chemical Soc. 71 (2024) 164–173.
[19] Q. Wang, H. Wei, Z. Zhang, E. Wang, S. Dong, Nanozyme: an emerging alternative to natural enzyme for biosensing and immunoassay, TrAC, Trends Anal. Chem. 105 (2018) 218–224.
[20] X. Meng, D. Li, L. Chen, H. He, Q. Wang, C. Hong, J. He, X. Gao, Y. Yang, B. Jiang, G. Nie, X. Yan, L. Gao, K. Fan, High-Performance self-cascade pyrite nanozymes for apoptosis-ferroptosis synergistic tumor therapy, ACS Nano 15 (2021) 5735–5751.
[21] D. Duan, K. Fan, D. Zhang, S. Tan, M. Liang, Y. Liu, J. Zhang, P. Zhang, W. Liu, X. Qiu, G.P. Kobinger, G. Fu Gao, X. Yan, Nanozyme-strip for rapid local diagnosis of Ebola, Biosens. Bioelectron. 74 (2015) 134–141.
[22] A.M. Villalba-Rodríguez, L.Y. Martínez-Zamudio, S.A.H. Martínez, J.A. Rodríguez-Hernández, E.M. Melchor-Martínez, E.A. Flores-Contreras, R.B. González-González, R. Parra-Saldívar, Nanomaterial constructs for catalytic applications in biomedicine: nanobiocatalysts and nanozymes, Top. Catal. 66 (2023) 707–722.
[23] N. Alizadeh, A. Salimi, Multienzymes activity of metals and metal oxide nanomaterials: applications from biotechnology to medicine and environmental engineering, J. Nanobiotechnol. 19 (2021) 26.
[24] L. Zhang, L. Zhang, H. Deng, H. Li, W. Tang, L. Guan, Y. Qiu, M.J. Donovan, Z. Chen, W. Tan, In vivo activation of pH-responsive oxidase-like graphitic nanozymes for selective killing of Helicobacter pylori, Nat. Commun. 12 (2021) 2002.
[25] J. Sun, Z. Wang, J. Guan, Single-atom nanozyme-based electrochemical sensors for health and food safety monitoring, Food Chem. 425 (2023) 136518.
[26] Q. Wang, H. Wei, Z. Zhang, E. Wang, S. Dong, Nanozyme: an emerging alternative to natural enzyme for biosensing and immunoassay, TrAC, Trends Anal. Chem. 105 (2018) 218–224.
[27] X. Chen, J. Liao, Y. Lin, J. Zhang, C. Zheng, Nanozyme’s catalytic activity at neutral pH: reaction substrates and application in sensing, Anal. Bioanal. Chem. 415 (2023) 3817–3830.
[28] K. Yu, M. Li, H. Chai, Q. Liu, X. Hai, M. Tian, L. Qu, T. Xu, G. Zhang, X. Zhang, MOF-818 nanozyme-based colorimetric and electrochemical dual-mode smartphone sensing platform for in situ detection of H_2O_2 and H_2S released from living cells, Chem, Eng. J. 451 (2023) 138321.
[29] H. Yue, L. Yuan, W. Zhang, S. Zhang, W. Wei, G. Ma, Macrophage responses to the physical burden of cell-sized particles, J. Mater. Chem. B 6 (2018) 393–400.
[30] J. Duncan, D. Sengupta, S. Bose, K.O. Kirlikovali, O.K. Farha, Defect-induced confinement in zirconium metal-organic frameworks for enhanced hydrogen adsorption, SCENV 3 (2023) 100032.
[31] T.A. Goetjen, A.J. Kropf, S. Alayoglu, M. Delferro, J.T. Hupp, O.K. Farha, Tuning the product distribution of acetylene dimerization through bimetallic metal-organic framework-supported nanoporous systems, ACS Appl. Nano Mater. 5 (2022) 14961–14969.
[32] H.-B. Luo, F.-R. Lin, Z.-Y. Liu, Y.-R. Kong, K.B. Idrees, Y. Liu, Y. Zou, O.K. Farha, X.-M. Ren, MOF-polymer mixed matrix membranes as chemical protective layers for solid-phase detoxification of toxic organophosphates, ACS Appl. Mater. Interfaces 15 (2023) 2933–2939.
[33] T. Li, J. Fang, X. Wan, H. Wang, L. Zhang, L. Wang, X. Qiu, G. Liang, Fe_3O_4@Ag@Pt nanoparticles with multienzyme like activity for total antioxidant capacity assay, Food Chem. 473 (2025) 143064.
[34] Z. Li, X. Hu, B. Li, X. Wang, Z. Shi, J. Lu, Z. Wang, MOF-derived Fe_3O_4 hierarchical nanocomposites encapsulated by carbon shells as high-performance anodes for Li-storage systems, J. Alloys Compd. 875 (2021) 159906.
[35] B. Bulut Kopuklu, A. Tasdemir, S. Alkan Gursel, A. Yurum, High stability graphene oxide aerogel supported ultrafine Fe_3O_4 particles with superior performance as a Li-ion battery anode, Carbon 174 (2021) 158–172.
[36] S. Hao, B. Zhang, Y. Wang, C. Li, J. Feng, S. Ball, M. Srinivasan, J. Wu, Y. Huang, Hierarchical three-dimensional Fe_3O_4@porous carbon matrix/graphene anodes for high performance lithium ion batteries, Electrochim. Acta 260 (2018) 965–973.
[37] J. Ouyang, Z. He, Y. Zhang, H. Yang, Q. Zhao, Trimetallic FeCoNi@C nanocomposite hollow spheres derived from metal-organic frameworks with superior electromagnetic wave absorption ability, ACS Appl. Mater. Interfaces 11 (2019) 39304–39314.
[38] G. Sun, H. Wu, Q. Liao, Y. Zhang, Enhanced microwave absorption performance of highly dispersed CoNi nanostructures arrayed on graphene, Nano Res. 11 (2018) 2689–2704.
[39] L. Wu, Y. Liu, H. Zhao, Z. Wang, B. Zhu, X. Zhang, P. He, Y. Liu, T. Yang, MOF-derived long spindle-like carbon-coated ternary transition-metal-oxide composite for lithium storage, ACS Omega 7 (2022) 16837–16846.
[40] X. Zhang, Q. Yang, Y. Lang, X. Jiang, P. Wu, Rationale of 3,3′,5,5′-Tetramethylbenzidine as the Chromogenic substrate in colorimetric analysis, Anal. Chem. 92 (2020) 12400–12406.